AGU PUBLICATIONS

JGR

Journal of Geophysical Research: Atmospheres

RESEARCH ARTICLE
10.1002/2015JD024067

Key Points:
- Investigate the influence of lateral subsurface flow connectivity on soil water storage
- Demonstrate subsurface flow variability effectively using lateral connectivity
- Develop a connectivity-based lateral subsurface flow algorithm in complex landscapes

Correspondence to:
B. P. Mohanty,
bmohanty@tamu.edu

Citation:
Kim, J., and B. P. Mohanty (2016), Influence of lateral subsurface flow and connectivity on soil water storage in land surface modeling, *J. Geophys. Res. Atmos.*, *121*, doi:10.1002/2015JD024067.

Received 19 AUG 2015
Accepted 19 DEC 2015
Accepted article online 23 DEC 2015

Influence of lateral subsurface flow and connectivity on soil water storage in land surface modeling

Jonggun Kim[1] and Binayak P. Mohanty[1]

[1]Department of Biological and Agricultural Engineering, Texas A&M University, College Station, Texas, USA

Abstract Lateral surface/subsurface flow and their connectivity play a significant role in redistributing soil water, which has a direct effect on biological, chemical, and geomorphological processes in the root zone (~1 m). However, most of the land surface models neglect the horizontal exchanges of water at the grid or subgrid scales, focusing only on the vertical exchanges of water as one-dimensional process. To develop better hydrologic understanding and modeling capability in complex landscapes, in this study we added connectivity-based lateral subsurface flow algorithms in the Community Land Model. To demonstrate the impact of lateral flow and connectivity on soil water storage we designed three cases including the following: (1) with complex surface topography only, (2) with complex surface topography in upper soil layers and soil hydraulic properties with uniform anisotropy. and (3) with complex surface topography and soil hydraulic properties with spatially varying anisotropy. The connectivity was considered as an indicator for the variation of anisotropy in the case 3, which was created by wetness conditions or geophysical controls (e.g., soil type, normalized difference vegetation index, and topographic index). These cases were tested in two study sites (ER 5 field and ER-sub watershed in Oklahoma) comparing to the field (gravimetric and remote sensing) soil moisture observations. Through the analysis of spatial patterns and temporal dynamics of soil moisture predictions from the study cases, surface topography was found to be a crucial control in demonstrating the variation of near surface soil moisture, but not significantly affected the subsurface flow in deeper soil layers. In addition, we observed the best performance in case 3 representing that the lateral connectivity can contribute effectively to quantify the anisotropy and redistributing soil water in the root zone. Hence, the approach with connectivity-based lateral subsurface flow was able to better characterize the spatially distributed patterns of subsurface flow and improve the simulation of the hydrologic cycle.

1. Introduction

Lateral surface/subsurface flow is an important hydrologic process and a key component of the water budget. Through its direct impacts on soil moisture, it can affect water and energy fluxes at the land surface and influence the regional climate and water cycle [*Gochis and Chen*, 2003; *Kumar*, 2004]. Further, the lateral flow and its connectivity play significant role in redistributing soil water, which have a direct effect on biological, chemical, and geomorphologic processes in the root zone [*Lu et al.*, 2011; *Western et al.*, 2001]. In spite of the importance of lateral flow, most of the land surface models (LSMs: Community Land Model (CLM), Noah Land Surface Model (Noah LSM), Variable Infiltration Capacity, etc.) neglect the horizontal exchanges of water at the grid or subgrid scales, focusing only on the vertical exchanges of water as a one-dimensional process. Surface routing models (e.g., River Transport Model, RTM) are already included to reflect the lateral movement of surface water in land surface modeling, but the lateral subsurface flow is excluded because the models generally assume that lateral transfers of subsurface moisture are fairly marginal in soil water budgets of a regional scale. Recently, 3-D hydrological surface-subsurface models were developed by coupling LSMs with distributed hydrological models to account for interactions between atmospheric, hydrological, and ecological processes (CATHY/NoahMP [*Niu et al.*, 2014] and PARFLOW/CLM [*Maxwell and Miller*, 2005]). Although these hydrological models include a process for the lateral subsurface flow, it still has limitations for deriving lateral hydraulic parameters (e.g., lateral hydraulic conductivity) that might be related to connected patterns of subsurface properties. Furthermore, spatial variability of soil moisture in the unsaturated zone cannot be described successfully without relevant understanding of how the subsurface flow is distributed or connected vertically or laterally in complex landscapes [*Hatton*, 1998; *Zhang et al.*, 1999; *Jana and Mohanty*, 2012a, 2012b, 2012c; *Shen et al.*, 2013]. More realistic understanding of surface and subsurface water movement at large scales can be also resolved through a hyperresolution land surface modeling that allows for better representation of spatially heterogeneous land surfaces [*Wood et al.*, 2011]. Thus, the lateral subsurface flow should be accounted for in hydrological modeling, characterizing vertical and lateral flow components effectively in the unsaturated zone.

Various studies have been conducted to account for the lateral flow in the unsaturated soil. *Zaslavsky and Sinai* [1981] explained a theory of unsaturated lateral flow with the major causes such as soil surface slope, anisotropy, and layering. *Famiglietti and Wood* [1994] developed a land surface modeling approach based on the TOPMODEL framework to address the impact of topographic configuration on soil moisture heterogeneity at a watershed scale. They showed a significant role of the topographic control in development of soil moisture heterogeneity and improved the simulation of hydrologic cycle using the modeling approach. *Chen and Kumar* [2001] explored the role of the topographic control in the seasonal and interannual variations of energy and water balances using statistical moments of topographic wetness indices and observed an improvement of streamflow predictions. Gravity and gradients in matric potential are also critical mechanisms in the unsaturated zone, causing soil water movements from high to low potential [*McCord and Stephens*, 1987; *Jana and Mohanty*, 2012a, 2012b, 2012c]. Water moving vertically through a heterogeneous soil profile can be influenced by the heterogeneity of soil hydraulic properties between soil layers, which can cause lateral flow at the interface [*Zhu and Lin*, 2009]. In process-based Soil-Vegetation-Atmosphere Transfer models, soil hydraulic properties (e.g., saturated soil water content, soil matric potential, and saturated hydraulic conductivity) are critical inputs to account for water movement in soil. The soil hydraulic properties are normally derived using several empirical equations (e.g., van Genuchten, Cosby, and Clapp and Hornberger) according to soil texture. Among the soil properties, an estimation of lateral hydraulic conductivity is more challenging because of the lack of available information. Thus, anisotropy has been used to derive the lateral hydraulic conductivities from the relationship between vertical and lateral permeability because soil behaves as an anisotropic medium which can cause lateral subsurface flow [*Zaslavsky and Sinai*, 1981; *Wang et al.*, 2011]. In the previous studies related to soil anisotropy, statistical or empirical anisotropy ratios were used at various scales [*Chen and Kumar*, 2001; *Kumar*, 2004; *Assouline and Or*, 2006; *Maxwell and Kollet*, 2008]. However, available experimental data and information for the anisotropy ratio in unsaturated soils might be limited to be applied in heterogeneous landscapes of large land areas. In order to overcome the limitations, the anisotropy ratio can be derived by spatially distributed patterns of wetness condition or its dominant physical controls such as soil texture, vegetation (*NDVI*), and topographic index (*TI*) to characterize the spatial pattern of subsurface flow in the unsaturated zone [*Chen and Kumar*, 2001].

A hydrologic connectivity has been proposed to address not only hydrologic flow paths but also spatial patterns of soil moisture variability at a catchment scale [*Western et al.*, 2001; *Hwang et al.*, 2009; *Gaur and Mohanty*, 2013]. The lateral connectivity is critically important for representing connected pathways of runoff in the landscapes and understanding movements of surface/subsurface flow [*Mueller et al.*, 2007; *Smith et al.*, 2010]. *Jencso et al.* [2009] derived hydrologic connectivity between catchment landscapes and channel network to identify runoff source areas based on the topographic characteristics. *Hwang et al.* [2012] found significant relationships between annual hydrologic metrics (e.g., runoff and evapotranspiration (ET)) and hydrologic vegetation gradient used as an indicator for lateral hydrologic connectivity at a watershed scale. Lateral subsurface flow connectivity can be derived from spatially distributed patterns of wetness condition or dominant physical factors and used to quantify the spatially varied anisotropy ratios in heterogeneous landscapes. In this study, we explored the influences of lateral subsurface flow and its connectivity on soil water storage in the unsaturated zone using a land surface model (Community Land Model (CLM)). None of previous studies have considered spatially varying anisotropy ratios derived from lateral connectivity to consider the lateral subsurface flow in hydrological modeling.

Thus, the objectives of this study are (1) to develop better hydrologic understanding and modeling capability in complex landscapes using a connectivity-based lateral subsurface flow algorithm and (2) to demonstrate the subsurface flow variability effectively using spatially distributed patterns of root zone wetness conditions and its physical controls at field and subwatershed scales. Although this study was focused on smaller-scale hydrological processes compared to large-scale climate models, it still can provide insights for large-scale land surface modeling to enhance their capability. In this study, the concept of lateral flow was used for the unsaturated zone that can be governed by topography and gradients in matric potential.

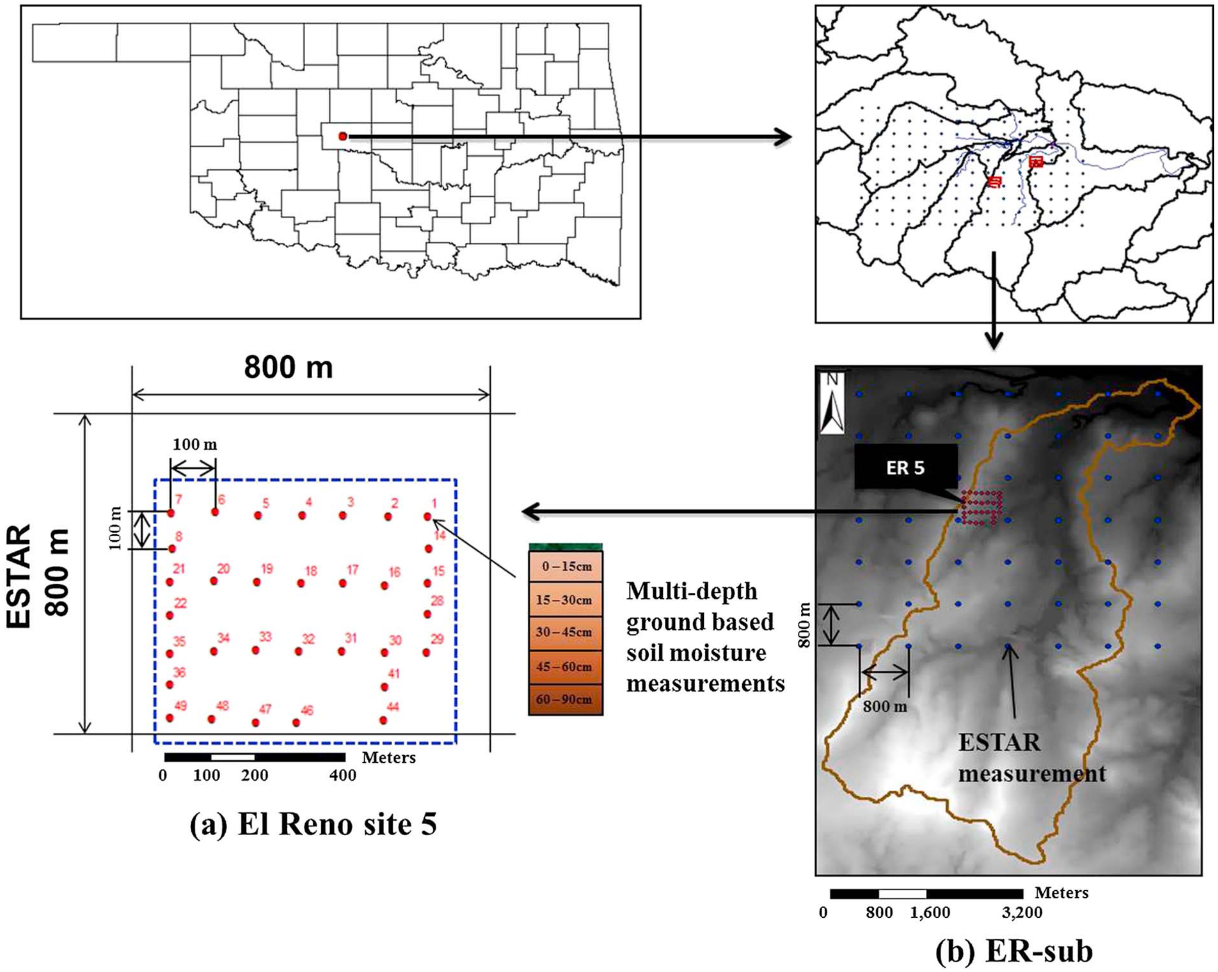

Figure 1. Study sites for (a) El Reno 5 (ER 5) matching the ESTAR remote sensing footprint with multidepth ground-based soil water measurements using truck-mounted Giddings probe (100 m spacing) and (b) El Reno subwatershed (ER-sub) in Oklahoma.

2. Methodology

2.1. Study Area

El-Reno site 5 (ER 5: field scale) and El-Reno subwatershed (ER-sub: subwatershed scale) located in North Canadian River basin in Oklahoma were selected to evaluate the proposed approach in this study (Figure 1). The ER 5 site (area: 0.8 km × 0.8 km) is located within the ER-sub boundary (area: 27 km^2). These sites have a sub-humid climate with an average annual rainfall of approximately 805 mm. Daily-mean maximum temperature is 34°C in July with annual-mean temperature of 15°C. The topography of the ER 5 is generally flat with average slopes less than 4.0%, while the ER-sub site has a variety of slopes from 11.0% to 0.001%. The ER 5 site has a native grass with 1 m root depth and mostly silty loam across the study domain. Vegetation in the ER-sub ranges from short and tall grasses (predominant) and forest in the north and central area to cropland in the south. Various soil types (e.g., silty loam (dominant), loam, and clay loam) are represented across the region.

Our proposed approach was validated with daily in situ soil moisture (49 sampling points) measured in top 5 cm soil (18 June to 17 July) and in depths of 0–15, 15–30, 30–45, 45–60, and 60–90 cm (6–15 July) during the Southern Great Plains experiment 1997 (SGP97) [*Mohanty et al.*, 2002] for the ER 5 site. Using a truck mounted Giddings probe, soil samples between the land surface and 90 cm depth were collected on a 7 × 7 square sampling grid (100 m spacing between sampling points) across the ER 5 field (Figure 1a). For the ER-sub site, we validated model predictions with Electronically Scanning Thin Array Radiometer (ESTAR) pixel-based (800 × 800 m) near surface soil moisture products [*Jackson et al.*, 1999] obtained during Southern Great Plains Experiment 1997, SGP97 (18 June to 17 July) (Figure 1b).

2.2. Description of Model Condition and Forcing Data

Community Land Model (CLM) [*Oleson et al.*, 2010] serves as the dynamic land surface model component of Community Earth System Model (CESM) [*Oleson et al.*, 2010], which consists of various processes such as biogeophysics, hydrologic cycle, biogeochemistry, and dynamic vegetation. The model can be run in off-line mode with prescribed forcing data or in a mode fully coupled to CESM with output from Community Atmosphere Model [*Collins et al.*, 2006], which is the atmospheric component of CESM. CLM simulates surface and subsurface runoff based on the simple TOPMODEL-based runoff model (SIMTOP) [*Niu et al.*, 2005]. The model considers water table dynamics as the lower boundary using the SIMple Groundwater Model (SIMGM) [*Niu et al.*, 2007]. Bare soil evaporation is simulated based on the *Philip and De Vries* [1957] diffusion model, and transpiration process uses an aerodynamic approach based on the Biosphere Atmosphere Transfer Scheme model [*Dickinson et al.*, 1993] and a stomatal resistance from the LSM model [*Bonan*, 1996]. River Transport Model (RTM) is coupled to CLM for the runoff routing process over a domain [*Oleson et al.*, 2010]. In this study, we used CLM4.0 and ran the model with RTM in off-line mode. The soil column in CLM consists of 10 soil layers with the thickness of 1.75, 2.76, 4.55, 7.5, 12.36, 20.38, 33.60, 55.39, 91.33, and 113.7 cm (total depth of 343 cm). Soil water flow in CLM is simulated by the modified one-dimensional (1-D) Richards' equation [*Zeng and Decker*, 2009]. CLM has been enhanced to improve hydrological cycle (water balance), vegetation dynamics, and computational performance in the last decade. Nevertheless, the model still simplify the complex processes for the root zone soil hydrology considering only vertical flow using 1-D Richards's equation. In this study, we modified soil water flow process including a lateral flow component in the unsaturated zone to improve the model performance (as described in section 2.3).

We run the model in off-line mode with atmospheric forcing data (precipitation, temperature, specific humidity, wind speed, surface air pressure, and solar radiation) collected from North American Land Data Assimilation System (NLDAS), which were applied uniformly for the study sites. In this study, we generated model input at spatial resolutions of 50 m and 100 m for the ER 5 site and the ER-sub, respectively. As required input data sets, land cover, soil types with depth, and topographic information were obtained from NLCD (National Land Cover Database), SSURGO (Soil Survey Geographic database), and NED (National Elevation Dataset), respectively. The bottom boundary condition of the model is decided with the water table dynamics calculated from aquifer water storage via the SIMGM [*Niu and Yang*, 2007], and then the model performed a spinning up to initialize the soil profile for the initial condition. In CLM, soil hydraulic properties are determined based on percentages of clay and sand using an empirical equation developed by *Clapp and Hornberger* [1978]. However, CLM tend to simulate the soil moisture lower than the observations in this study because the parameters estimated from the model input (percentages of clay and sand) for the ER 5 site were deviated from the referenced parameter ranges (Clapp and Hornberger table) of silty loam soil (predominant in the ER 5 site). Thus, we adjusted the parameters (trial and error) to satisfy the possible ranges of parameters and applied in CLM and modified CLM (section 2.3).

2.3. Lateral Subsurface Flow Process

CLM (based on one-dimensional simulation) assumes that soil water drains only vertically to the water table, and there are no interactions between parallel soil columns. To improve the simplified subsurface flow process in the unsaturated zone by CLM, we modified the one-dimensional vertical soil water flow with three-dimensional flow based on Richards's equation to consider the lateral subsurface flow in the model (Figure 1). The three-dimensional water flow can be expressed as follows,

$$\frac{\partial\theta}{\partial t} = -\frac{\partial q}{\partial X_c} - Q = \frac{\partial}{\partial X_c}\left[k_{X_c}\left(\frac{\partial\psi - \psi_E}{\partial X_c}\right)\right] - Q \tag{1}$$

where θ is the soil moisture content, t is time, q is the water flux in soil, X_c is $\{x,y,z\}$, x and y represent the horizontal directions, z represents the vertical direction, Q is a sink term (evapotranspiration (ET) loss), k_{Xc} is the unsaturated hydraulic conductivity in the direction X_c, ψ is the soil matric potential, and ψ_E is the equilibrium (E) soil matric potential, which means that there exists a constant hydraulic potential above the water table, when the water table is within the specified soil column/depth.

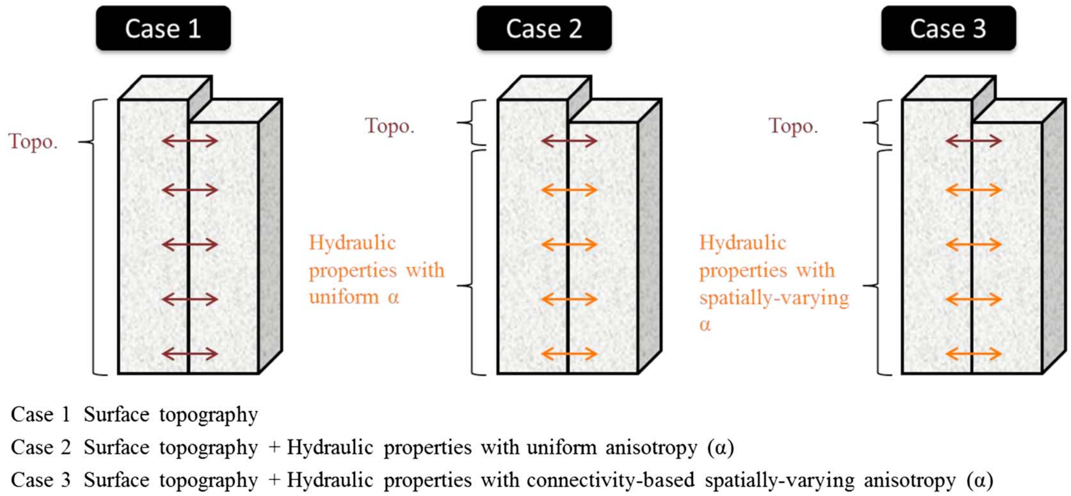

Figure 2. Three study cases designed for the lateral subsurface flow process. Anisotropy (α) is used to derive the saturated hydraulic conductivity in vertical and lateral directions as uniform (case 2) or connectivity-based spatially varying (case 3) ratio.

To estimate soil moisture content at each layer, the model solves a numerical solution based on equation (1). New lateral flow term (q_h) is added into the numerical solution of the model, and then the fluxes are calculated at time $n+1$ as follows,

$$\frac{\Delta X_{h,i}\Delta\theta_{h,i}}{\Delta t} = -q_{h-1,i-1}^{n+1} + q_{h,i}^{n+1} - Q_{h,i} \tag{2}$$

where $Q_{h,i}$ is a sink (e.g., ET loss) and h and i represent the number of soil columns (i.e., x and y direction) and layers (i.e., z direction), respectively.

The vertical and lateral fluxes in equation (2) are calculated as follows (equations (3) and (4)),

$$q_{h,i}^{n+1} = q_i^n + q_h^n + \frac{\partial q_i + \partial q_h}{\partial\theta_i}\Delta\theta_i + \frac{\partial q_i + \partial q_h}{\partial\theta_{i+1}}\Delta\theta_{i+1} \tag{3}$$

$$q_{h-1,i-1}^{n+1} = q_{i-1}^n + q_{h-1}^n + \frac{\partial q_{i-1} + \partial q_{h-1}}{\partial\theta_{i-1}}\Delta\theta_{i-1} + \frac{\partial q_{i-1} + \partial q_{h-1}}{\partial\theta_i}\Delta\theta_i \tag{4}$$

Let

$$q_{i-1}^n = -k_{V,i-1}\left[\frac{(\psi_{i-1}-\psi_i)+(\psi_{E,i}-\psi_{E,i-1})}{z_i - z_{i-1}}\right], \qquad q_i^n = -k_{V,i}\left[\frac{(\psi_i-\psi_{i+1})+(\psi_{E,i+1}-\psi_{E,i})}{z_{i+1}-z_i}\right],$$

$$q_{h-1}^n = -k_{H,h-1}\left[\frac{(\psi_{h-1}-\psi_h)}{x_h - x_{h-1}}\right], \qquad q_h^n = -k_{H,h}\left[\frac{(\psi_h-\psi_{h+1})}{x_{h+1}-x_h}\right].$$

where k_V and k_H represent vertical and lateral hydraulic conductivity (LT^{-1}), respectively.

To investigate the influences of lateral subsurface flow and its connectivity on soil water storage we designed three cases (Figure 2). Case 1 is to determine the lateral subsurface flow by slope of surface topography for all soil layers. In cases 2 and 3, the lateral subsurface flow is estimated by topography in the upper soil layers and heterogeneous hydraulic properties in the lower soil layers. One of the most challenging parameters in case 2 and 3 is lateral hydraulic conductivity (k_H), which should be identified appropriately to consider the lateral movement of soil water in the unsaturated zone. The term anisotropy was employed to derive the parameter (k_H) using uniform and spatially varying ratios (connectivity-based) for cases 2 and 3, respectively. Detailed explanations for each case are discussed in the following sections.

To evaluate the performance of modified model predictions for the study cases, we selected three performance criteria such as Pearson's correlation (R), root-mean-square error (RMSE), and mean absolute error (MAE).

2.3.1. Case 1: Topography

Surface topographic configuration plays a significant role in determining the soil water flow vertically and laterally near the surface indicating that the changes of flow direction based on the topography coincide with the changes in the rate of moisture content [*Chen and Kumar*, 2001; *Fan et al.*, 2007]. *Zaslavsky and Sinai* [1981] developed a simple relationship between the vertical and lateral component of soil water movement using the slope of surface topography and found that the lateral component was proportional to the slope and the vertical component of flow. In case 1, we assumed that the lateral subsurface flow moves parallel to the slope of surface topography. The lateral flux (q_h) can be estimated based on the relationship using surface slope as follows (equation (5)),

$$q_h = -k\left[\frac{\partial(\psi - \psi_E)}{\partial z}\right]\tan\beta \tag{5}$$

where β is the slope angle.

In addition, flow directions derived from digital elevation method using a single-direction algorithm (D8) in GIS hydrologic modeling were included to determine the direction of flow out of each soil column. Thus, the soil water flow process in CLM was modified using equation (7) with surface slope and flow direction for all soil layers to evaluate the influence of surface topography on the lateral subsurface flow in the unsaturated zone (Figure 2 (case 1)).

2.3.2. Case 2: Topography and Heterogeneous Hydraulic Properties With Uniform Anisotropy

Surface topography can be a dominant factor to determine the lateral component of subsurface flow near the slope surface, while the lateral subsurface flow in deep soil layers can be more influenced by heterogeneity of hydraulic properties [*Lu et al.*, 2011]. Thus, the two hydrologic processes (surface topography for 1st to 3rd layers and heterogeneous hydraulic properties for 4th to 10th layers) were considered together in case 2 (Figure 2). To take into account the lateral subsurface flow based on heterogeneous hydraulic properties, vertical and lateral hydraulic conductivity must be determined across a domain. However, the lateral hydraulic conductivity for spatially heterogeneous landscapes is unavailable and difficult to be measured, especially for large areas. Due to the limitations, an anisotropy ratio has been proposed to derive the saturated hydraulic conductivity in vertical and lateral directions that is defined as a directionally dependent property of soil [*Chen and Kumar*, 2001; *Choi et al.*, 2007]. The lateral saturated hydraulic conductivity ($K_{s,H}$) for each soil layer can be derived by multiplying the vertical saturated hydraulic conductivity ($K_{s,V}$) with the anisotropy ratio (α) as

$$K_{s,H}(z) = \alpha K_{s,V}(z) \tag{6}$$

The anisotropy ratio (α) can be obtained from published results or via model calibration through sensitivity analysis. In this study, we run the model adjusting the anisotropy ratio by trial and error within the possible ranges from literatures [*Chen and Kumar*, 2001] that compared to the soil moisture measurements for each depth. In turn, the appropriate ratio selected was applied to estimate the lateral hydraulic conductivity uniformly across the study sites in the modified CLM model.

2.3.3. Case 3: Topography and Heterogeneous Hydraulic Properties With Connectivity-Based Spatially Varying Anisotropy

In previous section, the anisotropy ratio (α) was applied with a constant value across the whole domain. However, anisotropy can be varied for different directions in accordance with various landscape conditions such as soil, vegetation, and topography configuration [*Chen and Kumar*, 2001]. In case 3, we added a connectivity-based lateral subsurface flow algorithm in subsurface process of CLM to quantify the spatially varying anisotropy ratio for the two study sites. A hydrologic connectivity is critically important for understanding spatial patterns of subsurface flow and can play a significant role in redistributing soil water in the unsaturated zone. It represents how a certain cell in a domain is connected to another cell through an indicator map. The indicator map (I) is used to identify the spatial patterns (connectivity) of interest variable (u, e.g., wetness condition or physical controls) above a threshold value (s) in the hydrologic connectivity process (equation (7)). The connectivity is calculated based on the indicator map using the connectivity function ($\tau(d)$) expressed as the probability that a certain cell (x) in a domain (X) is connected to another cell with a distance ($x + d$) in X (equatioin (8)).

$$I(u) = \begin{cases} 0 & if \quad u < s \\ 1 & if \quad u \geq s \end{cases} \tag{7}$$

$$\tau(d) = P(x \leftrightarrow x + d | x, x + d \in X) \tag{8}$$

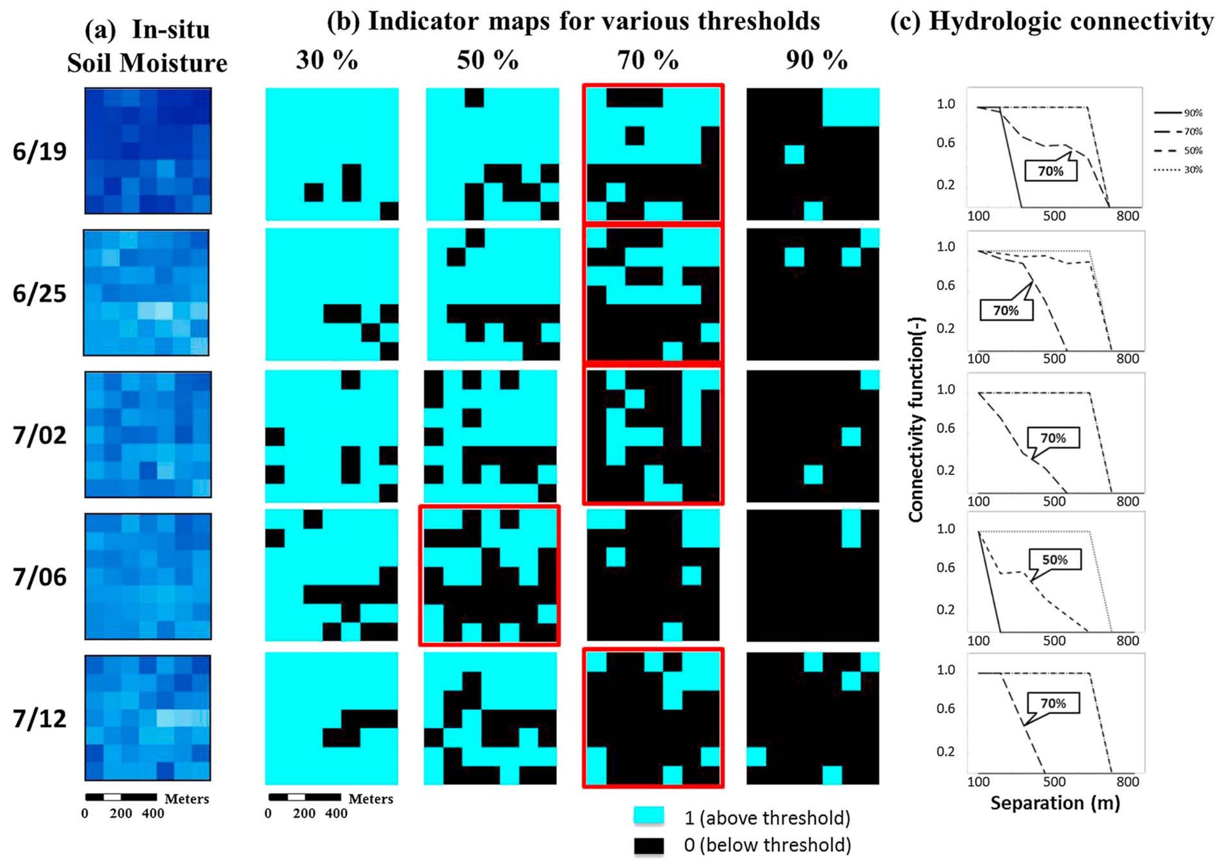

Figure 3. (a) In situ measurements at top 5 cm (pixel size: 100 × 100 m), (b) indicator maps for various thresholds of degree of soil wetness (θ/θ_s) on sampling dates, and (c) hydrologic connectivity for five sampling dates. Optimum threshold values for daily soil wetness were identified based on visual examination of the connectivity function versus separation distance plots. Note that selected red boxes around indicator maps correspond to the optimum thresholds selected from the connectivity functions, representing distinct connected patterns on various sampling dates.

Spatially varying anisotropy can be quantified using the lateral connectivity pattern derived by describing spatially distributed patterns of wetness conditions (e.g., soil moisture measurements) for the ER 5 site and various physical controls (e.g., soil type, vegetation, and topography) for the ER-sub site.

The connected patterns of wetness conditions above a certain threshold can be considered as preferred flow paths resulting from connected pixels or concentrated subsurface flow paths, assuming that higher wetness regions produce greater and faster flow in the unsaturated zone [*Western et al.*, 2001]. For the ER 5 site, the near surface soil moisture (~5 cm) observed on 5 days (19 and 25 June and 2, 6, and 12 July 1997) was used to investigate the spatial patterns of soil moisture (wetness) (Figure 3a). Indicator maps (binary maps coded 0 or 1) for four different thresholds of wetness (30, 50, 70, and 90%) were then created using the soil moisture measurements, indicating that pixels of soil moisture above the thresholds are assigned to "1" and others are assigned to "0" as shown in Figure 3b and Table 1. Using the indicator maps representing various connected patterns of soil moisture, we calculated the hydrologic connectivity for each map to find an optimum threshold value (or indicator map) that reflects the soil moisture connectivity well for the ER 5 site (Figure 3c) following the analysis in *Western et al.* [2001] study. The selected indicator maps for the

Table 1. Thresholds of Wetness of the Near Surface Soil Moisture Measurements for the ER 5 Site

	Thresholds of Wetness			
Date	30%	50%	70%	90%
19/6	0.40	0.44	0.48	0.53
25/6	0.23	0.29	0.35	0.41
02/7	0.30	0.34	0.39	0.44
06/7	0.31	0.35	0.38	0.42
12/7	0.26	0.32	0.38	0.44

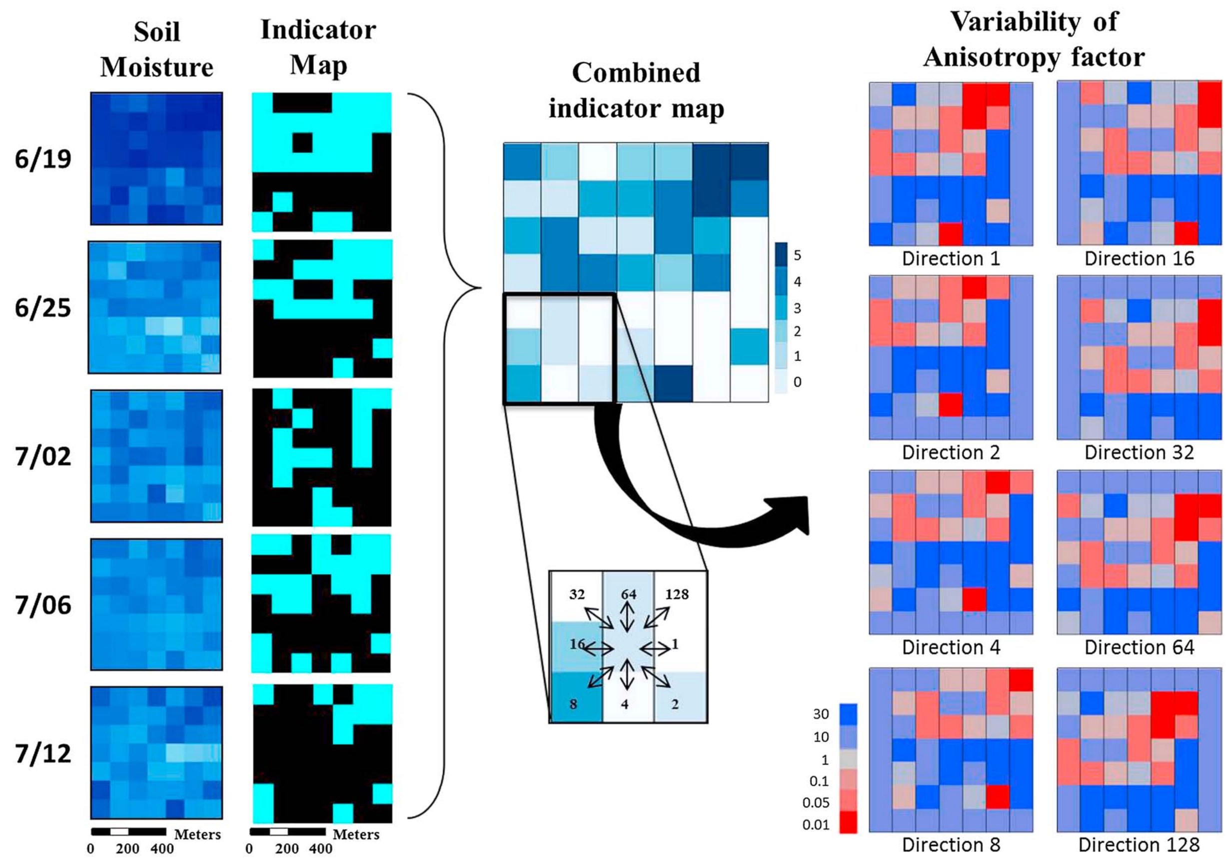

Figure 4. Spatially varying anisotropy ratio maps (pixel size: 100 × 100 m) (in eight directions) derived from the connectivity patterns for the near surface soil layers (1st to 3rd) by combining optimum indicator maps for all sampling dates. Similar maps of the other layers (not shown) were derived from the soil moisture measured at deeper soils (up to 90 cm).

5 days (red boxes in Figure 3b) were combined to consider the possible patterns from the different measurement days and determine how the lateral flow can be distributed across the domain. In turn, we derived spatially varying anisotropy ratio maps in eight directions through assigning the ratios ranging from 30 to 0.01 according to the combined indicator map ranging from 0 to 5 (Figure 4). The possible ranges of the anisotropy ratio were obtained from literatures, and the numerical experiments conducted in previous section for the study site. In general, hydraulic conductivity in lateral directions is higher than that in vertical directions, but this is not always true because the unsaturated zone is highly complex with various flow processes such as preferential flow (macropore flow), which might cause soil water movement quickly in vertical direction ($\alpha < 1$) [*Dabney and Selim*, 1987]. The spatially varying anisotropy ratio maps for the upper soil layers (1st to 3rd layers) were generated using the near surface soil moisture measurement. For the deep soil layers (4th ~ 10th), the anisotropy ratios were derived from the soil profile measurements (0–15, 15–30, 30–45, 45–60, and 60–90 cm) in a similar way. However, the measurements for deep soil are available only for 2 days (6 and 15 July) during the SGP 97 campaign period. Thus, indicator maps for five thresholds of wetness (40, 50, 60, 70, and 80%) were estimated (Table 2) and combined by adding their binary values to represent the spatially distributed soil moisture patterns and quantify the anisotropy ratios. The spatially varying anisotropy ratios were then estimated based on the combined map for each soil layer.

Table 2. Thresholds of Wetness of the Root Zone Soil Moisture Measurements With Depth for the ER 5 Site

	Thresholds of Wetness				
Depth	40%	50%	60%	70%	80%
0–15	0.35	0.38	0.41	0.45	0.48
15–30	0.30	0.31	0.33	0.34	0.35
30–45	0.21	0.24	0.27	0.29	0.32
45–60	0.32	0.34	0.35	0.36	0.38
60–90	0.25	0.27	0.30	0.32	0.34

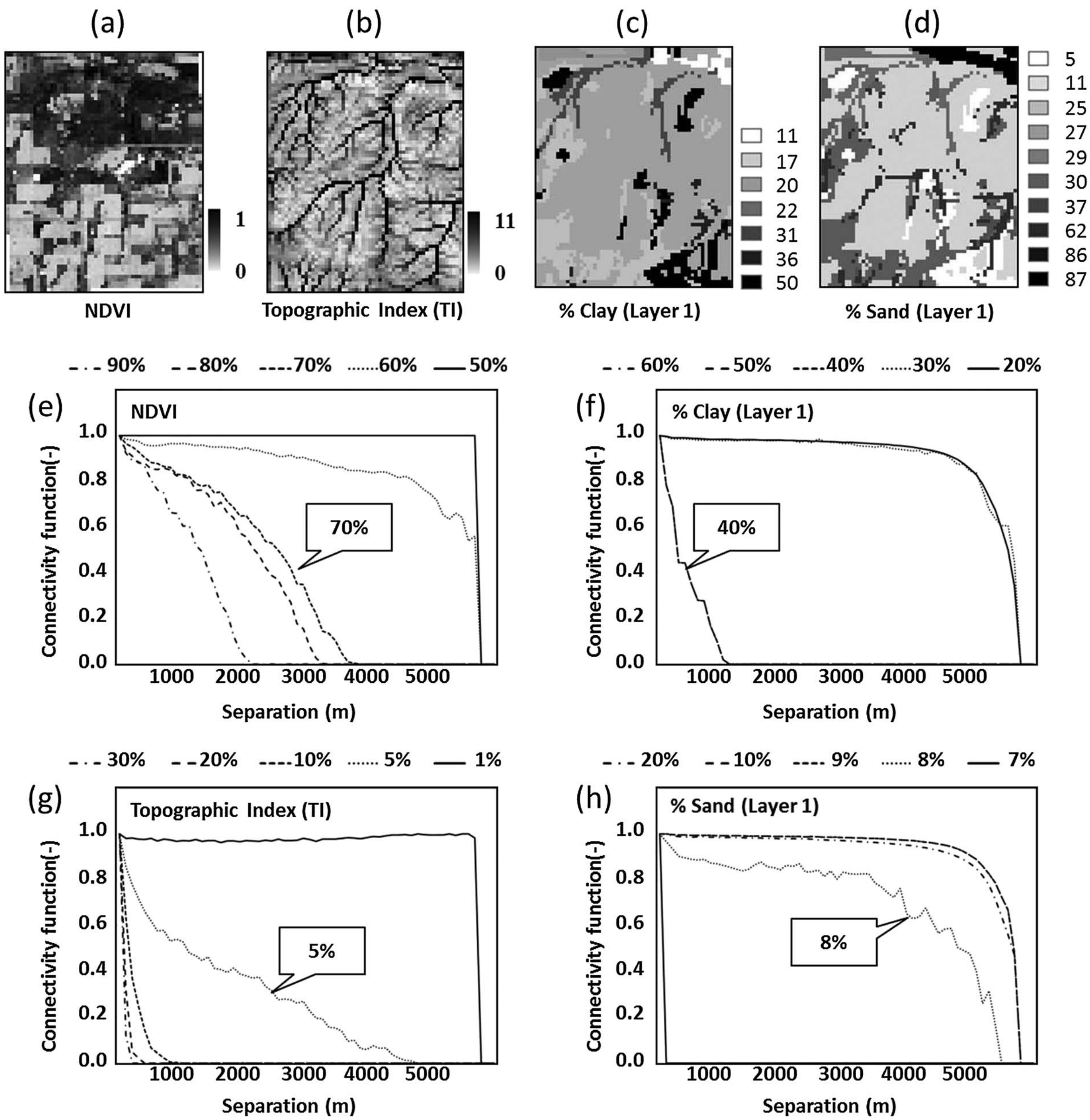

Figure 5. Dominant physical controls ((a) NDVI, (b) %clay, (c) %sand, and (d) topographic index) and (e–f) their connectivity functions for the ER-sub site. Thresholds values for different physical controls were defined based on its range and numerical analyses. Optimum threshold values for individual physical controls were identified based on visual examination of the connectivity function versus separation distance plots.

Thus, the lateral component of subsurface flow was calculated using the anisotropy ratios in the modified CLM for the ER 5 site.

In addition to the wetness condition (soil moisture), various physical controls such as soil, vegetation, and topographic configuration have been identified as dominant controls on the variability of soil moisture at watershed scales [*Mohanty and Skaggs*, 2001; *Joshi and Mohanty*, 2010; *Gaur and Mohanty*, 2013]. These factors can also be used to describe how soil water flows and redistributes in heterogeneous landscapes with regard to the anisotropy. For example, the clay content in soil has a significant effect on anisotropy due to its low permeability retaining more water in soil. Root density in vegetation area could also be related to anisotropy in soil, leading to nonuniform lateral hydraulic conductivity [*Yang and Musiake*, 2003]. The spatial pattern of vegetation density within a watershed is a good estimator for spatial patterns of root zone moisture dynamics and lateral connectivity within watersheds [*Hwang et al.*, 2009]. In this study, soil moisture

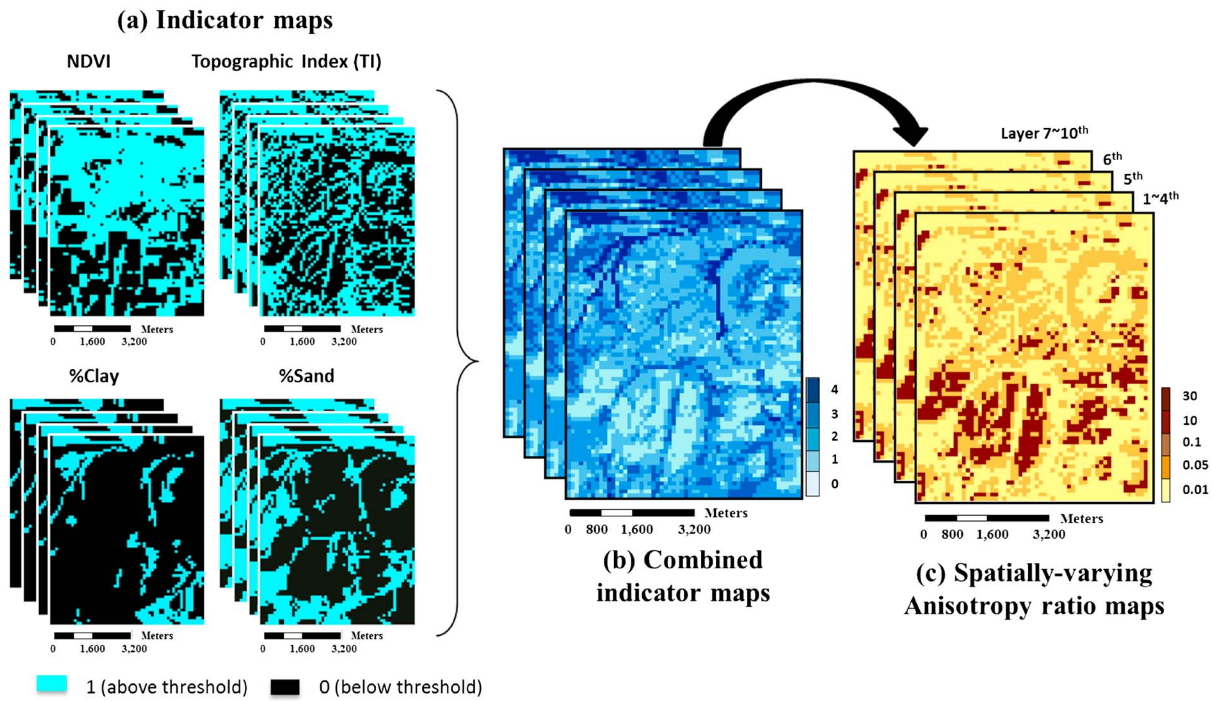

Figure 6. (a) Optimum indicator maps of various physical controls (NDVI, TI, %clay, and %sand) for various soil layers (1st–10th), (b) combined indicator maps for each soil layer, and (c) corresponding spatially varying anisotropy ratio maps (pixel size: 100 × 100 m) at the ER-sub site.

measurements with depth are not available for the ER-sub site; hence, we derived the subsurface connectivity patterns using the dominant physical controls (percentage of clay and sand, NDVI, and topographic index) for quantifying the anisotropy ratios (Figures 5a–5d). Recent studies explored the combined effects of topography and vegetation on connectivity of runoff source areas and shallow groundwater and showed the potential for improving the estimation of hydrologic connectivity [*Mayor et al.*, 2008; *Hwang et al.*, 2009; *Emanuel et al.*, 2014]. Thus, we considered connected patterns of the combination of physical controls as landscape descriptors or potential predictors for redistribution of soil moisture in the unsaturated zone. Using the connectivity function (equation (8)), we found an optimum threshold for each variable reflecting connected patterns across the ER-sub site (Figures 5e–5h) and generated their indicator maps using equation (9). In turn, the indicator maps for the physical controls were combined to reflect the effects of physical controls jointly on hydrological processes that represents unique configurations of the physical components like the concept of hydrological response units [*Flügel*, 1995] as expressed in equation (9).

$$\text{CombinedMap} = I(\%\text{clay}) + I(\%\text{sand}) + I(\text{NDVI}) + I(\text{TI}) \tag{9}$$

where I(%clay), I(%sand), I(NDVI), and I(TI) represent the indicator maps (binary maps) for the percentage of clay and sand, NDVI ((R_{NIR}-R_{red})/($R_{\text{NIR}} + R_{\text{red}}$)), and topographic index (TI, Ln(a/tanβ)), respectively; R_{NIR} and R_{red} are the reflectance of near infrared (NIR) radiation and visible red radiation, respectively; a represents the upslope area; and tanβ is the local downslope. The physical controls may not contribute equally to describing the soil moisture variability in the unsaturated zone, but in this study we assumed that the variables have equal effects on hydrological processes because it is difficult to identify which physical control contributes more to the redistribution of subsurface soil moisture that can vary with complex landscape characteristics. The spatially varying anisotropy ratio maps for each soil layer were then estimated for the ER-sub (Figure 6) and applied in the modified CLM model to estimate the lateral component of subsurface flow.

3. Results and Discussions

CLM was modified through three different cases designed in this study taking into account the effects of lateral subsurface flow and its connectivity on soil water storage in the unsaturated zone. In order to validate

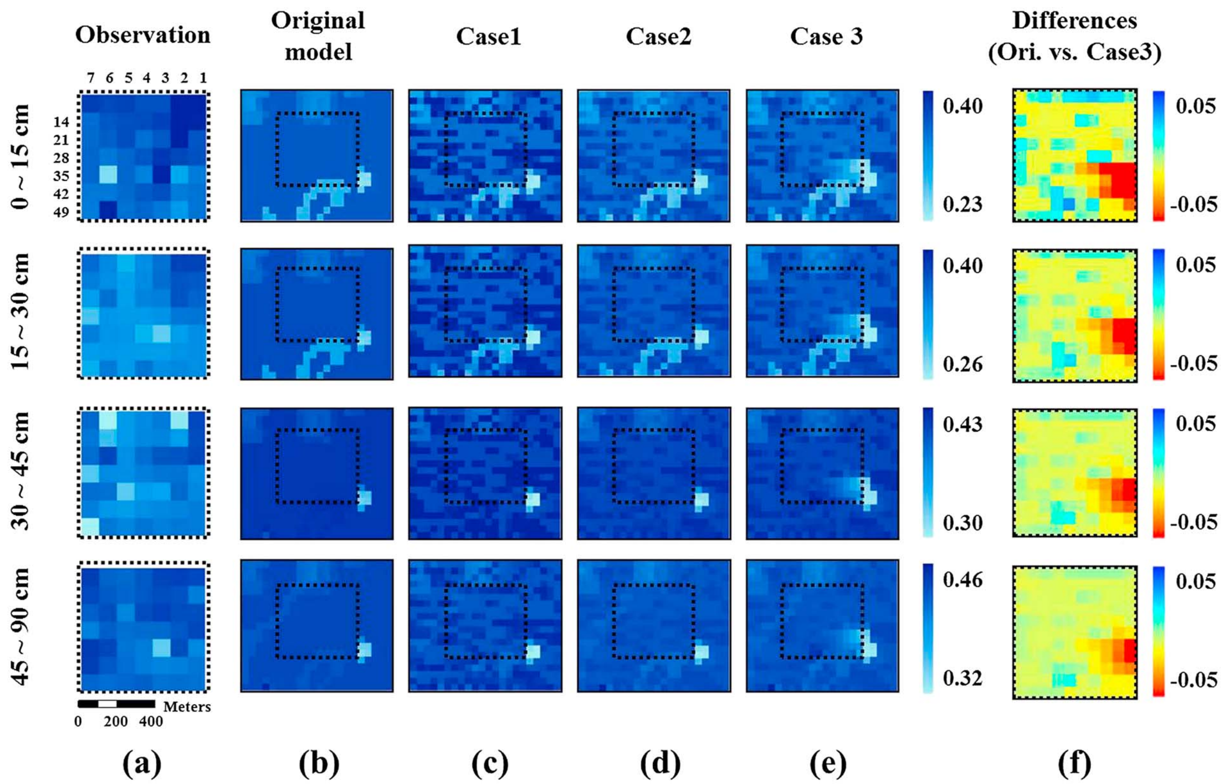

Figure 7. Comparison of the root zone soil moisture of (a) ground observation (pixel size: 100 × 100 m), (b) original CLM model, and modified CLM model (pixel size: 50 × 50 m) through (c) case 1, (d) case 2, and (e) case 3 at the ER 5 site, and (f) differences between the original and modified CLM model of case 3.

the proposed approach, the simulated near surface and root zone (up to 90 cm) soil moisture using the modified CLM model in the three cases were compared to that of original CLM model and observations at the two study sites (field and subwatershed scale).

3.1. Field Scale (El-Reno Site 5)

Near surface and root zone soil moisture was simulated using the modified model including the lateral subsurface flow based on three different cases at the ER 5 site. Figure 7 shows the comparison of observed and simulated root zone soil moisture using the original model and modified model for the three cases with depth (0–15, 15–30, 30–45, and 45–90 cm) on 6 July 1997. Although the study site has almost uniform land cover and soil type, the observations for all depths showed the variability in the soil moisture distribution that can be attributed to the influence of lateral subsurface flow (Figure 7a). However, the original model output represented almost uniform patterns across the site because one-dimensional model estimates the root zone soil moisture identically under the same input data (e.g., vegetation and soil), ignoring the interactions between soil columns (Figure 7b). When we included the lateral flow component based on the slope, the modified model (case 1) showed spatially distributed soil moisture patterns indicating higher moisture content on the area of low elevation (Figure 7c). This was because the modified model simulated the root zone soil moisture considering that soil water flows from the upstream to the downstream according to the flow direction as the lateral subsurface flow. We also confirmed an improvement of describing the soil moisture variability with the lateral subsurface flow in Figure 8a, which shows the comparisons of simulated root zone soil moisture using the original and modified model against the observations with depth. The original model showed the uniform patterns of root zone soil moisture across the domain, while the modified model (case 1) showed the variation in root zone soil moisture indicating small improvement compared to the original model, especially at the depth of 0–30 cm. Based on the results of case 1, we found that the subsurface flow prediction can be improved by considering the lateral subsurface flow based on the topography, but there was still uncertainty predicting the root zone soil moisture in deep soil layers (30–45 and 45–90 cm) causing overestimations for the study site. It can be inferred that considering the surface topography only is not

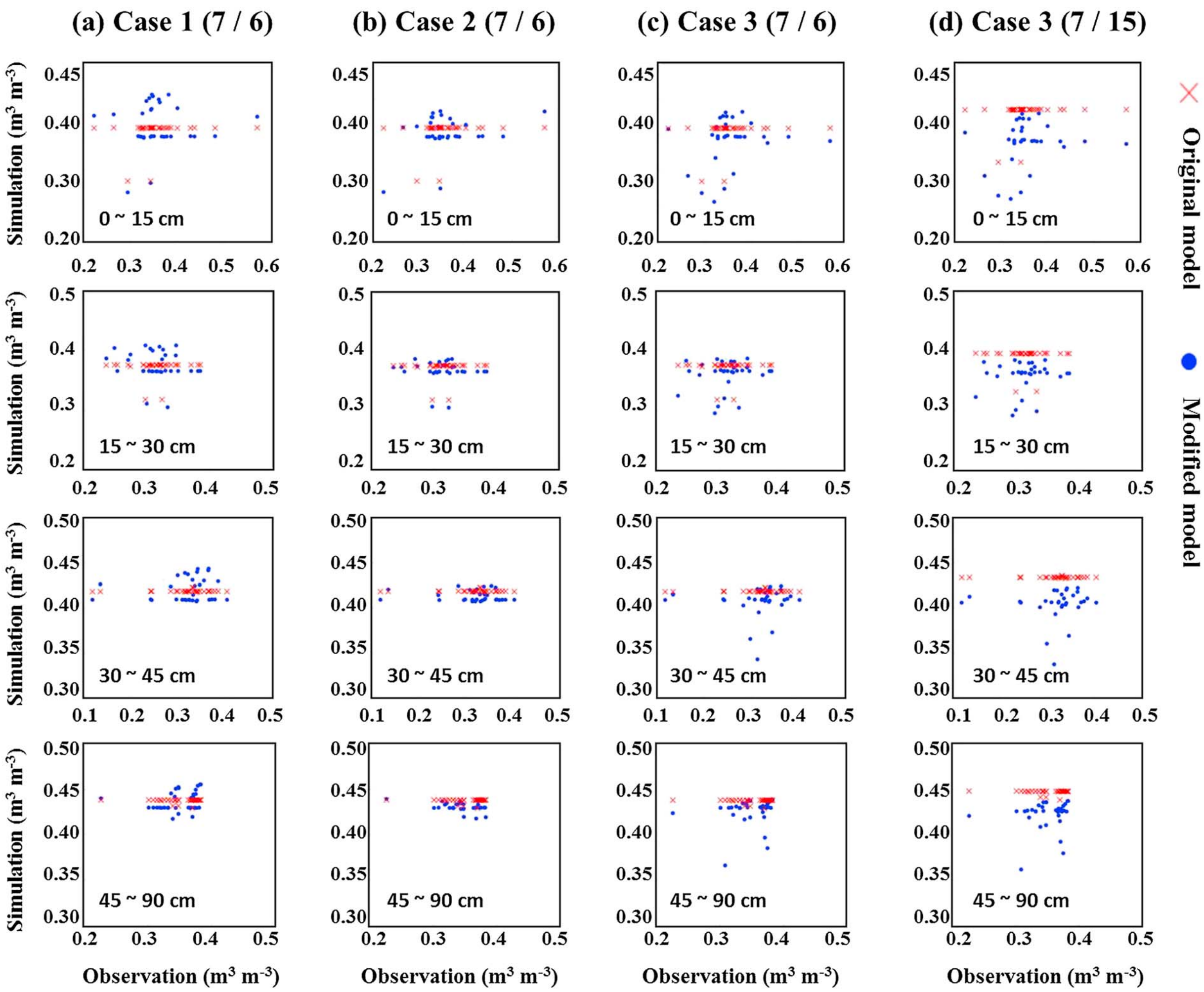

Figure 8. Comparison of the simulated root zone soil moisture using the original and modified model against the observations; (a) case 1, (b) case 2, and (c) case 3 in July 6th and (d) case 3 in July 15th for the ER 5 site.

enough to account for the root zone soil moisture variability in deep soil because surface and subsurface topography may differ and the lateral subsurface flow in deep soil layers may be governed more by heterogeneous hydraulic properties.

In case 2, the lateral flow component was estimated by topography for the upper layer (1st to 3rd) and heterogeneous hydraulic properties with uniform anisotropy for the lower layers (4th to 10th) together. In this study, we performed the numerical experiments to find a proper (optimum) anisotropy ratio (α) within the possible range (0.01–30) for the study site. When the anisotropy ratio of 0.05 was applied, the model output (soil moisture with depth) was most similar to the observations through the numerical experiments for the ER 5 site. The ratio was applied uniformly across the domain to estimate the lateral hydraulic conductivity. The modified model (case 2) also predicted the root zone soil moisture better than the original model (Figure 7d). Figure 8b shows the predicted root zone soil moisture using the modified model against the multidepth ground-based observation for all the grid cells. The results of the case 2 were slightly improved than that of case 1, indicating that the average model predictions were closer to the observations. The root zone soil moisture predicted in case 1 (considering surface topography only) tend to be overestimated in all depths, while the modified model including heterogeneous hydraulic properties with uniform anisotropy ratio showed better performance. This is because high moisture content in certain grid cells can be redistributed effectively into the neighboring cells depending on the heterogeneous hydraulic properties of soil as a lateral subsurface flow. Although case 2 showed more improvement for predicting near surface soil moisture variability (0–30 cm), it could not capture the soil moisture patterns in deep soil layers using the uniform anisotropy ratio (Figure 8b).

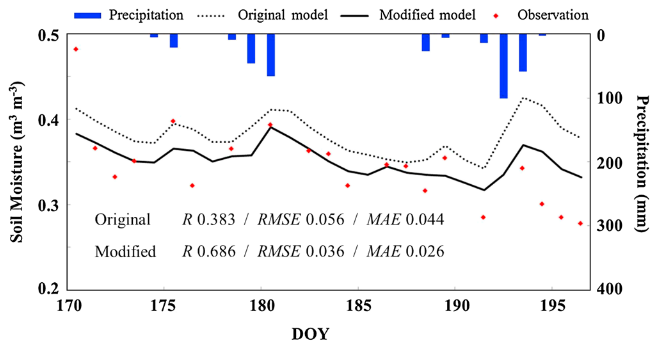

Figure 9. Comparison of observed and simulated (case 3) near surface soil moisture dynamics (top 5 cm) using original (dotted line) and modified model (black line) at the ER 5 site.

In previous studies, an anisotropy ratio has been applied uniformly in a domain to calculate the lateral component of subsurface flow [*Chen and Kumar*, 2001; *Kumar*, 2004; *Choi et al.*, 2007]. However, we found that the lateral flow component using the constant anisotropy ratio could not identify the subsurface flow successfully in deep soil at the ER 5 site.

In order to overcome the limitations observed in cases 1 and 2, the spatially varying anisotropy ratios were derived from the observed soil moisture patterns (wetness) through the hydrologic connectivity and the optimal thresholds as mentioned in section 2.3.3. Figures 7e and 8c show the comparison of observed and simulated root zone soil moisture across the study site with depth for 6 July 1997. Compared to the cases 1 and 2 with no connectivity, the results of the case 3 with connectivity presented better performances to predict the root zone soil moisture patterns within the domain, even showing improvement in deeper soil layers (30–45 and 45–90 cm). The improvement was also confirmed with a validation in 15 July 1997 (Figure 8d) representing better agreement with the variability of observations than the original model. It can be inferred that the lateral connectivity derived from the wetness conditions can describe the spatial patterns of subsurface flow effectively with quantifying the spatially varying anisotropy ratios. The lateral subsurface flow resulted in the differences between original and modified model prediction that might lead to affect the simulation of the hydrological cycle and various components significantly (Figure 7f).

Furthermore, we compared the simulated near surface soil moisture dynamics using the case 3 (day of year 170–197) with in situ measurements. To compare the observation and simulation, soil moisture data across the domain were averaged to match the grid-based predictions with point-scale observations. The modified model of case 3 (R: 0.686, $RMSE$: 0.036, and MAE: 0.026) improved the near surface soil moisture predictions more than the original model (R: 0.383, $RMSE$: 0.056, and MAE: 0.044) (Figure 9). Based on these results for the ER 5 site, it was found that the lateral component of subsurface flow in the unsaturated zone is considerably important for predicting soil water storage successfully in land surface modeling and can be derived with the connectivity-based lateral subsurface flow algorithm. In addition, we can quantify the spatially varying anisotropy ratios effectively and characterize the lateral subsurface flow variability using the connectivity patterns derived from wetness conditions and geophysical controls in the unsaturated zone.

3.2. Subwatershed Scale (El-Reno Subwatershed)

As shown in the previous section (field scale), we confirmed that the modified model with subsurface connectivity (quantifying the spatially varying anisotropy ratios) performed better at ER-sub site than the original model and the case with spatially uniform anisotropy ratio. Further, we validated the modified model (case 3) in the ER-sub site located in North Canadian River basin to investigate the impacts of the lateral subsurface flow and its connectivity on water storage in soil at a much larger scale. The observed and predicted output was compared with their spatial patterns and temporal dynamics.

Figure 10 presents the comparison of the simulated near surface and root zone soil moisture measured at discrete depths using the original and modified CLM model. Compared to the remotely sensed ESTAR observations (0–5 cm), the original CLM model has a limitation in describing the soil moisture variability without lateral subsurface flow (Figure 10a). The model also tend to overestimate the soil moisture and predicted identical soil water content in grid cells having the same soil type and vegetation due to the limitation of 1-D model. On the other hand, with the connectivity-based lateral subsurface flow the soil moisture prediction was improved representing spatially distributed patterns in all depths (Figure 10b). The connectivity with depth was derived from the combination of indicator maps (corresponding to their optimum thresholds selected using the connectivity function) of the dominant physical controls (%clay, %sand, NDVI, and TI). It was found that the connected pattern based on the various physical controls can provide significant

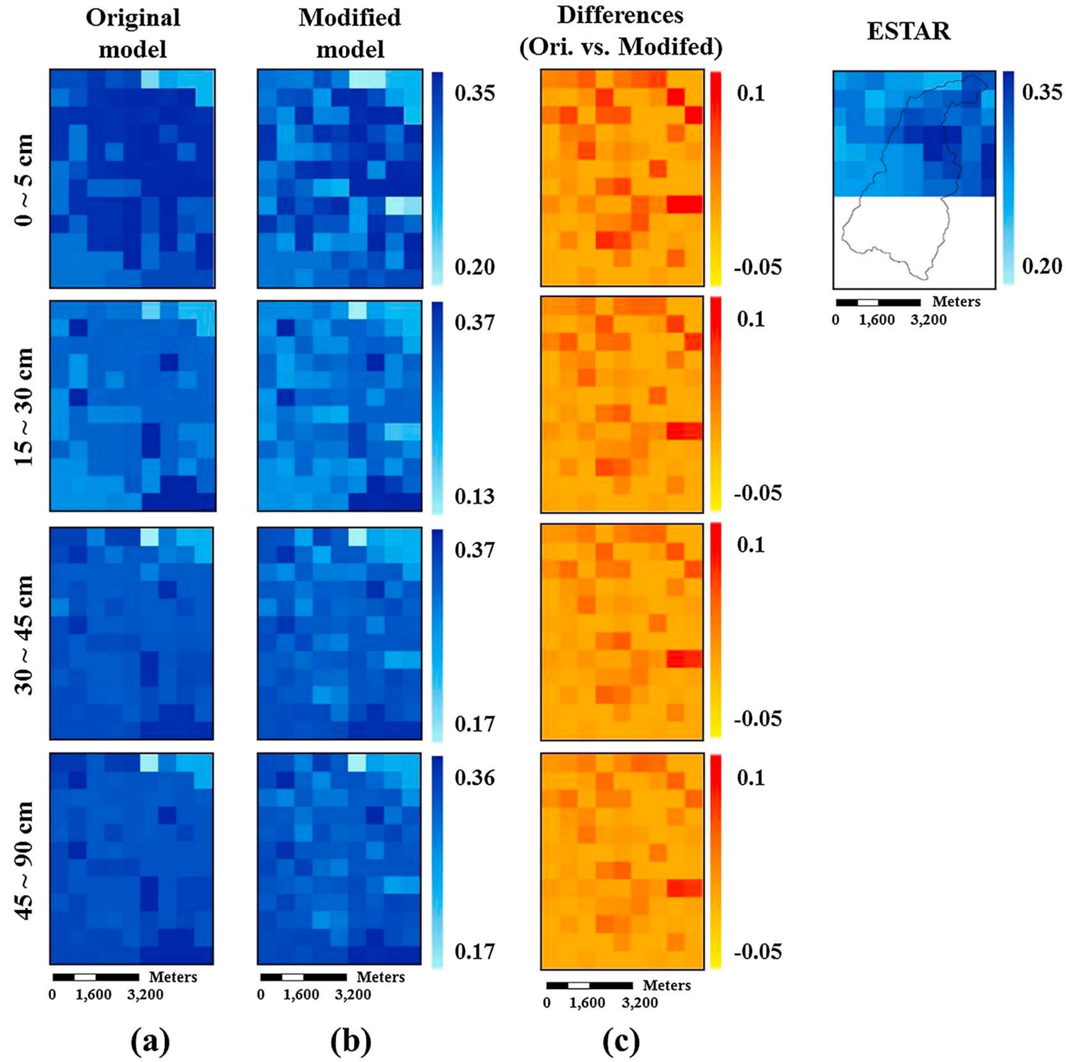

Figure 10. Comparison of the root zone soil moisture (pixel size: 800 × 800 m) at various depths of (a) original model and (b) modified model (case 3), and (c) their differences for the ER-sub site.

hydrologic behaviors of subsurface flow to demonstrate the variability of subsurface flow and allow the model to redistribute soil water effectively at the ER-sub site. To assess their similarity of spatial patterns quantitatively, the model output was compared to the observations through spatial moving window analysis, which is useful to assess spatial patterns. Several different window sizes (1 × 1, 2 × 2, 3 × 3, and 4 × 4) were selected, and the average of model output within the moving window was used to measure the spatially distributed patterns. For 1 × 1 window size, the results of the three model evaluation criteria (*R*, *RMSE*, and *MAE*) were too low, although the modified model showed better performances than the original model (Original CLM model —*R*: 0.30, *RMSE*: 0.090, and *MAE*: 0.083; Modified CLM model—*R*: 0.33, *RMSE*: 0.076, and *MAE*: 0.066). This was because the low values of model evaluation criteria were affected by mismatch between the same grid cells, even though they could be in close agreement at coarser scale (with neighboring grid cells).

Table 3. Comparison of Spatial Patterns of Simulated Near Surface Soil Moisture Using the Original and Modified Model With Various Spatial Moving Window Sizes

	1 × 1			2 × 2			3 × 3			4 × 4		
	R	RMSE	MAE	R	RMSE	MAE	R	RMSE	MAE	R	RMSE	MAE
Original CLM	0.30	0.090	0.083	0.34	0.076	0.084	0.43	0.086	0.083	0.35	0.084	0.082
Modified CLM (case 3)	0.33	0.076	0.066	0.47	0.069	0.065	0.63	0.067	0.065	0.60	0.065	0.064

	R	RMSE	MAE
Original	0.88	0.089	0.077
Modified (case 3)	0.90	0.076	0.065

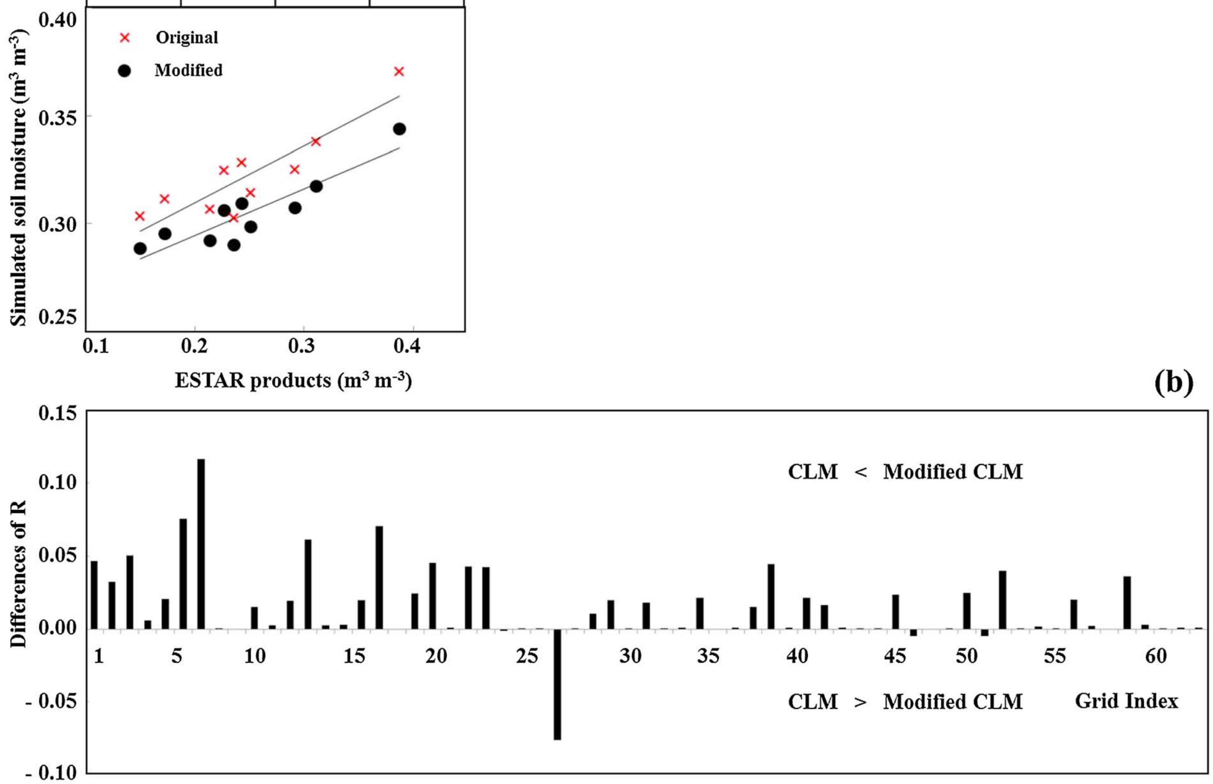

Figure 11. Comparison of the simulated near surface soil moisture for (a) the average within the ER-sub site against ESTAR observations and (b) the differences of R values for each grid cell.

As the window size increases, the similarity of modified model output increased showing improvements in the model prediction (Table 3). Overall, the spatial patterns could not be matched exactly in fine scale; however, the model was able to describe the variability of soil moisture through the connectivity-based lateral subsurface flow. As shown in Figure 11a, the modified model showed better agreement with the ESTAR observations (*R*: 0.90, *RMSE*: 0.076, and *MAE*: 0.065) than the original model (*R*: 0.88, *RMSE*: 0.089, and *MAE*: 0.077). Although the comparison is based on average soil moisture, it can be inferred that the lateral subsurface flow based on connectivity between subgrid cells within a large grid cell could enhances the modeling skill at large scales. Furthermore, in order to demonstrate the spatial and temporal comparisons within the subwatershed, we calculated the differences of *R* values of soil moisture dynamics between the original and modified model (Figure 11b) in all grid cells. The positive difference (+) mean that the modified model performed better than original model in the grid cell. The results in most of the grid cells showed that the modified model with the connectivity-based lateral subsurface flow can predict the soil water content better spatially and temporally in the ER-sub watershed.

As shown in the comparison of spatial patterns and temporal dynamics of soil moisture prediction, there are differences between the model predictions with and without the lateral subsurface flow in land surface modeling, giving rise to the different soil water storage in the unsaturated zone (Figure 10c). In land surface modeling, soil moisture is an important component that affects considerably other components of the land surface water cycle (e.g., evapotranspiration, surface runoff, and subsurface drainage) due to the interactions between them. The differences of soil moisture prediction between the original and modified model led to significantly different surface runoff, subsurface drainage, and water storage (soil water + groundwater) (Figure 12).

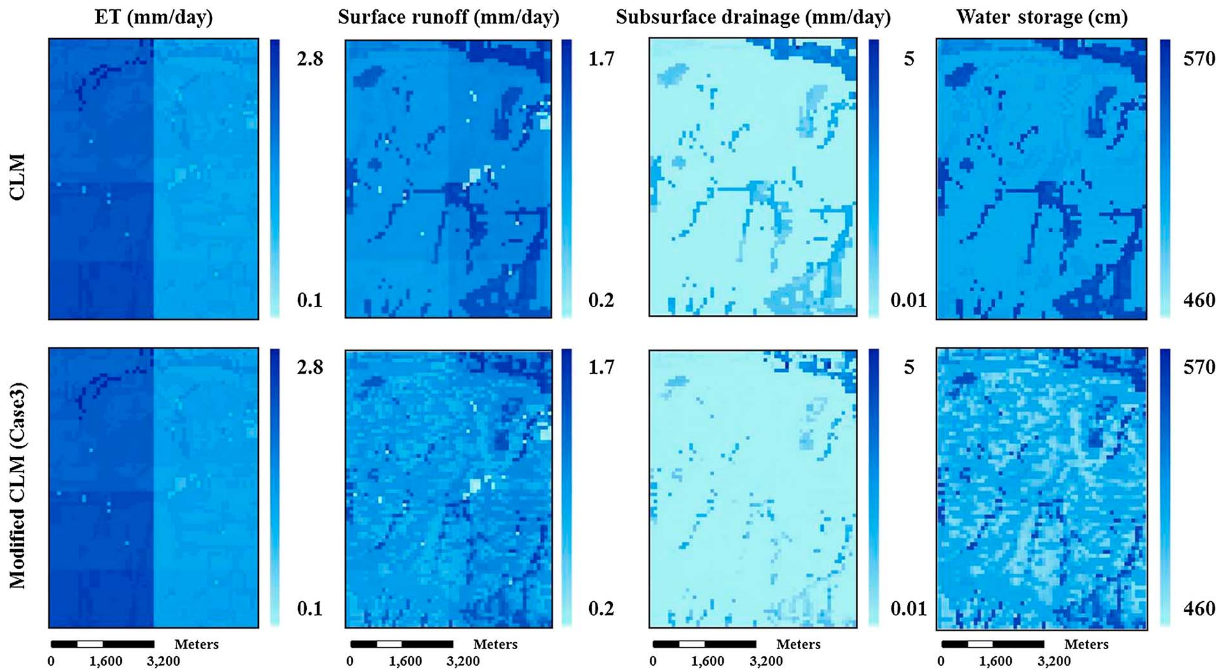

Figure 12. Simulated evapotranspiration (ET), surface runoff, subsurface drainage, and water storage using the original and modified model (pixel size: 100 × 100 m) at the ER-sub site.

4. Summary and Conclusions

Most of the land surface models are one-dimensional, which is not enough to explain the soil moisture variability in the root zone due to absence of interaction (lateral flow) between neighboring soil columns. There is a need to consider the lateral subsurface flow properly in hydrological modeling to account for spatially distributed soil moisture effectively and improve the prediction of subsurface redistribution of flow. Slope of surface topography and heterogeneity of hydraulic properties are considered to include the lateral subsurface flow in the unsaturated zone. One of the important factors is anisotropy ratio used for estimating the lateral hydraulic conductivity that varies spatially according to various landscape conditions such as wetness, soil, vegetation, and topographic configuration. The spatially varying anisotropy ratios can be derived using a lateral connectivity pattern from wetness conditions and physical controls because the connectivity is a useful concept for understanding spatially distributed lateral subsurface flow and redistributing soil water in the unsaturated zone. In order to investigate the impacts of lateral subsurface flow and its connectivity on soil water storage, in this study we designed three cases (case 1—surface topography; case 2—topography and heterogeneous hydraulic properties with uniform anisotropy; case 3—topography and heterogeneous hydraulic properties with spatially varying anisotropy derived from connectivity patterns).

In ER 5 field site, the model predictions in case 1 showed the similar patterns to the observed near surface soil moisture distribution but could not successfully describe the root zone soil moisture patterns in deep soils. It suggests that the surface topography may not contribute to the lateral subsurface flow in deep soil at the site. The modified model in the case 2 also performed better than that in the case 1 and original model representing a good agreement with the observations. Nevertheless, the case 2 with uniform anisotropy ratio could not still capture the soil moisture variability in deep soil. On the other hands, the model prediction in the case 3 using the spatially varying anisotropy ratio derived from the connectivity showed more improvements in all soil layers. We found that the connectivity derived from the wetness conditions could characterize the spatial patterns of lateral subsurface flow effectively and quantify the spatially varying anisotropy ratio properly.

The modified CLM model with connectivity-based lateral subsurface flow (case 3) was validated at a subwatershed site (ER-sub). The connectivity patterns were developed using the spatial patterns of physical controls (e.g., %sand, %clay, NDVI, and TI) to quantify the spatially varying anisotropy ratio in this ER-sub site. The modified CLM model improved further the soil moisture prediction than the original CLM model leading to significant differences in performance between the models.

Based on these findings, we infer that the modified model with connectivity can characterize effectively the subsurface flow variability using spatially distributed patterns of wetness condition and physical controls. However, we also found limitations of the approach for deriving anisotropy ratio (α) and wetness connectivity due to their site-specific characteristics. The parameter and wetness connectivity obtained from combining indicator maps of various physical controls (assuming that the variables have equal effects on hydrological processes) may not be applicable in other sites such as forested or low-lying areas. The limitations can be addressed to improve the applicability of the approach in future works by reflecting effectively on site specific characteristics (i.e., dominant physical controls) in various landscapes and climate regions. Although this study has such limitations and was focused on relatively small-scale hydrological processes compared to large-scale climate models (e.g., $1° \times 1°$), these processes can be helpful to develop better understanding and modeling capability with the connectivity-based lateral subsurface flow in complex landscapes and allows for an improved simulation of the hydrologic cycle.

Acknowledgments
This research was funded by NASA THP-NNX09AK73G and NSF DMS-09-34837 grants. Multidepth ground-based soil water measurements (contact person: Binayak P. Mohanty (bmohanty@tamu.edu) at Texas A&M University) and ESTAR remote sensing footprint used in this study were collected from Southern Great Plains experiment 1997 (SGP97, contact person: Michael H. Cosh (michael.cosh@ars.usda.gov) at USDA-ARS Hydrology and Remote Sensing Lab). Weather data sets were obtained from North American Land Data Assimilation System (NLDAS, http://ldas.gsfc.nasa.gov/nldas/NLDASnews.php). The required input data sets (land cover, soil types, and topographic information) were collected from NLCD (National Land Cover Database, http://www.mrlc.gov/), SSURGO (Soil Survey Geographic database, http://www.nrcs.usda.gov/wps/portal/nrcs/detail/soils/survey/geo/?cid=nrcs142p2_053631), and NED (National Elevation Dataset, http://ned.usgs.gov/), respectively.

References

Assouline, S., and D. Or (2006), Anisotropy factor of saturated and unsaturated soils, *Water Resour. Res.*, *42*, W12403, doi:10.1029/2006WR005001.

Bonan, G. B. (1996), A land surface model (LSM version 1.0) for ecological, hydrological, and atmospheric studies: Technical description and user's guide, *NCAR Tech. Note NCAR/TN-417+STR*, 150 pp.

Chen, J., and P. Kumar (2001), Topographic influence on the seasonal and inter-annual variation of water and energy balance of basins in North America, *J. Clim.*, *14*, 1989–2014.

Choi, H. I., P. Kumar, and X.-Z. Liang (2007), Three-dimensional volume-averaged soil moisture transport model with a scalable parameterization of subgrid topographic variability, *Water Resour. Res.*, *43*, W04414, doi:10.1029/2006WR005134.

Clapp, R. B., and G. M. Hornberger (1978), Empirical equations for some soil hydraulic properties, *Water Resour. Res.*, *14*, 601–604, doi:10.1029/WR014i004p00601.

Collins, W. D., P. J. Rasch, B. A. Boville, J. J. Hack, J. R. McCaa, D. L. Williamson, B. P. Briegleb, C. M. Bitz, S.-J. Lin, and M. Zhang (2006), The formulation and atmospheric simulation of the Community Atmosphere Model Version 3 (CAM3), *J. Clim.*, *19*, 2144–2161.

Dabney, S. M., and H. M. Selim (1987), Anisotropy of a fragipan soil: Vertical vs. horizontal hydraulic conductivity, *Soil Sci. Soc. Am. J.*, *51*, 3–6.

Dickinson, R. E., A. Henderson-Sellers, and P. J. Kennedy (1993), Biosphere atmosphere transfer scheme (BATS) version 1e as coupled to the NCAR Community Climate Model, *NCAR Tech. Note*, *NCAR/TN-378+STR*, Natl. Cent. For Atmos. Res., Boulder, Colo.

Emanuel, R. E., A. G. Hazen, B. L. McGlynn, and K. G. Jencso (2014), Vegetation and topographic influences on the connectivity of shallow groundwater between hillslopes and streams, *Ecohydrology*, *7*, 887–895, doi:10.1002/eco.1409.

Famiglietti, J. S., and E. F. Wood (1994), Multiscale modeling of spatially variable water and energy balance processes, *Water Resour. Res.*, *30*, 3061–3078.

Fan, Y., G. Miguez-Macho, C. P. Weaver, R. Walko, and A. Robock (2007), Incorporating water table dynamics in climate modeling: 1. Water table observations and equilibrium water table simulations, *J. Geophys. Res.*, *112*, D10125, doi:10.1029/2006JD008111.

Flügel, W. A. (1995), Delineating Hydrological Response Units (HRUs) by GIS analysis regional hydrological modelling using PRMS/ MMS in the drainage basin of the River Bröl, Germany, *Hydrol. Processes*, *9*, 423–436.

Gaur, N., and B. P. Mohanty (2013), Evolution of physical controls for soil moisture in humid and subhumid watersheds, *Water Resour. Res.*, *49*, 1244–1258, doi:10.1002/wrcr.20069.

Gochis, D. J. and F. Chen (2003), Hydrological enhancements to the community Noah land surface model, *NCAR Tech. Note NCAR/TN-454+STR*, 68 pp.

Hatton, T. J. (1998), *The Basics of Recharge and Discharge, Part 4, Catchment Scale Recharge Modeling*, Commonw. Sci. and Ind. Res. Organ., Collingwood, Victoria, Australia.

Hwang, T., L. Band, and T. C. Hales (2009), Ecosystem processes at the watershed scale: Extending optimality theory from plot to catchment, *Water Resour. Res.*, *45*, W11425, doi:10.1029/2009WR007775.

Hwang, T., L. E. Band, J. M. Vose, and C. Tague (2012), Ecosystem processes at the watershed scale: Hydrologic vegetation gradient as an indicator for lateral hydrologic connectivity of headwater catchments, *Water Resour. Res.*, *48*, W06514, doi:10.1029/2011WR011301.

Jackson, T. J., D. M. Le Vine, A. Y. Hsu, A. Oldak, P. J. Starks, C. T. Swift, J. D. Isham, and M. Haken (1999), Soil moisture mapping at regional scales using microwave radiometry: The Southern Great Plains hydrology experiment, *IEEE Trans. Geosci. Remote Sens.*, *37*, 2136–2151.

Jana, R. B., and B. P. Mohanty (2012a), On topographic controls of soil hydraulic parameter scaling at hillslope scales, *Water Resour. Res.*, *48*, W02518, doi:10.1029/2011WR011204.

Jana, R. B., and B. P. Mohanty (2012b), A topography-based scaling algorithm for soil hydraulic parameters at hillslope scales: Field testing, *Water Resour. Res.*, *48*, W02519, doi:10.1029/2011WR011205.

Jana, R. B., and B. P. Mohanty (2012c), A comparative study of multiple approaches to soil hydraulic parameter scaling applied at the hillslope scale, *Water Resour. Res.*, *48*, W02520, doi:10.1029/2010WR010185.

Jencso, K. G., B. L. McGlynn, M. N. Gooseff, S. M. Wondzell, K. E. Bencala, and L. A. Marshall (2009), Hydrologic connectivity between landscapes and streams: Transferring reach- and plot-scale understanding to the catchment scale, *Water Resour. Res.*, *45*, W04428, doi:10.1029/2008WR007225.

Joshi, C., and B. P. Mohanty (2010), Physical controls of near surface soil moisture across varying spatial scales in an agricultural landscape during SMEX02, *Water Resour. Res.*, *46*, W12503, doi:10.1029/2010WR009152.

Kumar, P. (2004), Layer averaged Richard's equation with lateral flow, *Adv. Water Resour.*, *27*(5), 521–531.

Lu, N., B. S. Kaya, and J. W. Godt (2011), Direction of unsaturated flow in a homogeneous and isotropic hillslope, *Water Resour. Res.*, *47*, W02519, doi:10.1029/2010WR010003.

Maxwell, R. M., and S. J. Kollet (2008), Quantifying the effects of three-dimensional subsurface heterogeneity on Hortonian runoff processes using a coupled numerical, stochastic approach, *Adv. Water Resour.*, *31*, 807–817, doi:10.1016/j.advwatres.2008.01.020.

Maxwell, R. M., and N. L. Miller (2005), Development of a coupled land surface and groundwater model, *J. Hydrometeorol.*, *6*(3), 233–247.

Mayor, Á. G., S. Bautista, E. E. Small, M. Dixon, and J. Bellot (2008), Measurement of the connectivity of runoff source areas as determined by vegetation pattern and topography: A tool for assessing potential water and soil losses in drylands, *Water Resour. Res.*, *44*, W10423, doi:10.1029/2007WR006367.

McCord, J. T., and D. B. Stephens (1987), Lateral moisture flow beneath a sandy hillslope without an apparent impeding layer, *Hydrol. Processes*, *1*, 225–238.

Mohanty, B. P., and T. H. Skaggs (2001), Spatio-temporal evolution and time-stable characteristics of soil moisture within remote sensing footprints with varying soil, slope, and vegetation, *Adv. Water Resour.*, *24*, 1051–1067.

Mohanty, B. P., P. J. Shouse, D. A. Miller, and M. T. Van Genuchten (2002), Soil property database: Southern Great Plains 1997 hydrology experiment, *Water Resour. Res.*, *38*(5), 1047, doi:10.1029/2000WR000076.

Mueller, E. N., J. Wainwright, and A. J. Parsons (2007), Impact of connectivity on the modeling of overland flow within semiarid shrubland environments, *Water Resour. Res.*, *43*, W09412, doi:10.1029/2006WR005006.

Niu, G.-Y., and Z.-L. Yang (2007), An observation-based formulation of snow cover fraction and its evaluation over large North American river basins, *J. Geophys. Res.*, *112*, D21101, doi:10.1029/2007JD008674.

Niu, G.-Y., Z.-L. Yang, R. E. Dickinson, and L. E. Gulden (2005), A simple TOPMODEL-based runoff parameterization (SIMTOP) for use in GCMs, *J. Geophys. Res.*, *110*, D21106, doi:10.1029/2005JD006111.

Niu, G.-Y., Z.-L. Yang, R. E. Dickinson, L. E. Gulden, and H. Su (2007), Development of a simple groundwater model for use in climate models and evaluation with Gravity Recovery and Climate Experiment data, *J. Geophys. Res.*, *112*, D07103, doi:10.1029/2006JD007522.

Niu, G.-Y., C. Paniconi, P. A. Troch, R. L. Scott, M. Durcik, X. Zeng, T. Huxman, and D. C. Goodrich (2014), An integrated modelling framework of catchment-scale ecohydrological processes: 1. Model description and tests over an energy-limited watershed, *Ecohydrology*, *7*, 427–439.

Oleson, K. W., D. M. Lawrence, G. B. Bonan, M. G. Flanner, E. Kluzek, P. J. Lawrence, S. Levis, S. C. Swenson, and P. E. Thornton (2010), Technical sescription of version 4.0 of the Community Land Model (CLM), *NCAR Tech. Notes (NCAR/TN-478+STR)*, 257 pp.

Philip, J. R., and D. de Vries (1957), Moisture movement in porous materials under temperature gradients, *Eos Trans. AGU*, *38*, 222–232.

Shen, C., J. Niu, and M. S. Phanikumar (2013), Evaluating controls on coupled hydrologic and vegetation dynamics in a humid continental climate watershed using a subsurface-land surface processes model, *Water Resour. Res.*, *49*, 2552–2572, doi:10.1002/wrcr.20189.

Smith, M. W., L. J. Bracken, and N. J. Cox (2010), Toward a dynamic representation of hydrological connectivity at the hillslope scale in semiarid areas, *Water Resour. Res.*, *46*, W12540, doi:10.1029/2009WR008496.

Wang, X.-. S., X.-. W. Jiang, L. Wan, S. Ge, and H. Li (2011), A new analytical solution of topography-driven flow in a drainage basin with depth-dependent anisotropy of permeability, *Water Resour. Res.*, *47*, W09603, doi:10.1029/2011WR010507.

Western, A. W., G. Bloschl, and R. B. Grayson (2001), Toward capturing hydrologically significant connectivity in spatial patterns, *Water Resour. Res.*, *37*, 83–97.

Wood, E. F., et al. (2011), Hyperresolution global land surface modeling: Meeting a grand challenge for monitoring Earth's terrestrial water, *Water Resour. Res.*, *47*, W05301, doi:10.1029/2010WR010090.

Yang, D., and K. Musiake (2003), A continental scale hydrological model using the distributed approach and its application to Asia, *Hydrol. Processes*, *17*, 2855–2869.

Zaslavsky, D., and G. Sinai (1981), Surface hydrology: I. Explanation of phenomena, *J. Hydraul. Div. Am. Soc. Civ. Eng.*, *107*, 1–16.

Zeng, X. B., and M. Decker (2009), Improving the numerical solution of soil moisture-based Richards equation for land models with a deep or shallow water table, *J. Hydrometeorol.*, *10*, 308–319.

Zhang, L., W. R. Dawes, T. J. Hatton, P. H. Reece, G. T. H. Beale, and I. Packer (1999), Estimation of soil moisture and groundwater recharge using the TOPOG_IRM model, *Water Resour. Res.*, *35*, 149–161.

Zhu, Q., and H. S. Lin (2009), Simulation and validation of concentrated subsurface lateral flow paths in an agricultural landscape, *Hydrol. Earth Syst. Sci.*, *13*, 1503–1518.